Title

Target-selectivity of parvalbumin-positive interneurons in layer II of medial entorhinal cortex in normal and epileptic animals

Journal

Hippocampus, 26(6)

ISSN

1050-9631

Authors

Armstrong, Caren

Wang, Jessica

Yeun Lee, Soo

et al.

Publication Date

2016-06-01

DOI

10.1002/hipo.22559

Peer reviewed

HHS Public Access

Author manuscript

Hippocampus. Author manuscript; available in PMC 2017 June 01.

Published in final edited form as:

Hippocampus. 2016 June ; 26(6): 779–793. doi:10.1002/hipo.22559.

Target-Selectivity of Parvalbumin-Positive Interneurons in Layer II of Medial Entorhinal Cortex in Normal and Epileptic Animals

Caren Armstrong[1,2], **Jessica Wang**[1], **Soo Yeun Lee**[1,3], **John Broderick**[1], **Marianne J Bezaire**[1,4], **Sang-Hun Lee**[1,5], and **Ivan Soltesz**[6,1]

[1]University of California, Irvine Department of Anatomy & Neurobiology

[6]I. Soltesz: Department of Neurosurgery, Stanford University

Abstract

The medial entorhinal cortex layer II ($MEC_{layerII}$) is a brain region critical for spatial navigation and memory, and it also demonstrates a number of changes in patients with, and animal models of, temporal lobe epilepsy (TLE). Prior studies of GABAergic microcircuitry in $MEC_{layerII}$ revealed that cholecystokinin-containing basket cells (CCKBCs) select their targets on the basis of the long-range projection pattern of the postsynaptic principal cell. Specifically, CCKBCs largely avoid reelin-containing principal cells that form the perforant path to the ipsilateral dentate gyrus and preferentially innervate non-perforant path forming calbindin-containing principal cells. We investigated whether parvalbumin containing basket cells (PVBCs), the other major perisomatic targeting GABAergic cell population, demonstrate similar postsynaptic target selectivity as well. In addition, we tested the hypothesis that the functional or anatomic arrangement of circuit selectivity is disrupted in $MEC_{layerII}$ in chronic TLE, using the repeated low-dose kainate model in rats.

In control animals, we found that PVBCs innervated both principal cell populations, but also had significant selectivity for calbindin-containing principal cells in $MEC_{layerII}$. However, the magnitude of this preference was smaller than for CCKBCs. In addition, axonal tracing and paired recordings showed that individual PVBCs were capable of contacting both calbindin and reelin-containing principal cells.

In chronically epileptic animals, we found that the intrinsic properties of the two principal cell populations, the GABAergic perisomatic bouton numbers, and selectivity of the CCKBCs and PVBCs remained remarkably constant in $MEC_{layerII}$. However, miniature IPSC frequency was decreased in epilepsy, and paired recordings revealed the presence of direct excitatory connections between principal cells in the $MEC_{layerII}$ in epilepsy, which is unusual in normal adult $MEC_{layerII}$. Taken together, these findings advance our knowledge about the organization of perisomatic inhibition both in control and in epileptic animals.

Corresponding Author Information: Caren Armstrong, 139 Irvine Hall, Department of Anatomy & Neurobiology, University of California, Irvine School of Medicine, Irvine, CA 92697-1280, (303)548-1187 (cell), cmarmstr@uci.edu.

[2]C Armstrong current address: Department of Pediatrics, Johns Hopkins Hospital;

[3]SY Lee current address: Department of Bioengineering, Stanford University;

[4]M. Bezaire current address: Department of Psychological and Brain Sciences, Boston University;

[5]S-H Lee current address: Department of Neurology, University of Arkansas for Medical Sciences;

Keywords

Calbindin; Reelin; Perisomatic inhibition; Basket cell; MEC

Introduction

Medial Entorhinal Cortical Layer II Microcircuits and Projections

Layer II of the medial entorhinal cortex ($MEC_{layerII}$) is an important part of a distributed network for spatial navigation and memory processing (Deng, 2009; Hafting et al., 2005; Mizuseki et al., 2009; Solstad et al., 2008) and gives rise to the perforant path, which terminates in the molecular layer of the dentate gyrus (Steward, 1976; van Strien et al., 2009). Two distinct populations of principal cells coexist in $MEC_{layerII}$, distinguishable on the basis of their immunoreactivity to either reelin (Chin et al., 2007; Ramos-Moreno et al., 2006) or calbindin (Fujimaru and Kosaka, 1996; Varga et al., 2010). Previously, using retrograde tracers, it was shown that reelin-containing principal cells ($reelin^+$) projected to the ipsilateral dentate gyrus via the perforant path while calbindin-containing principal cells ($calb^+$) were found to project to other, non-dentate brain regions (including, but likely not limited to, the contralateral entorhinal cortex) (Kitamura et al., 2014; Kohara et al., 2014; Ramos-Moreno et al., 2006; Ray et al., 2014; Rowland et al., 2013; Steward and Scoville, 1976; van Strien et al., 2009; Varga et al., 2010). This unique separation by immunolabeling enables the identification of principal cells in $MEC_{layerII}$ with distinct projection patterns using immunohistochemical markers (Ray et al., 2014; Varga et al., 2010).

In addition to different projection patterns, these two principal cell types were found to differentially receive input from the cholecystokinin positive basket cells (CCKBCs) (Varga et al., 2010). Perisomatically-targeting GABAergic basket cells innervating the somata of principal cells are separable into two distinct classes: parvalbumin containing (PV) and cholecystokinin containing (CCK), which have different intrinsic properties, sensitivities to neuromodulators, and network roles in both neocortical and hippocampal networks (Armstrong and Soltesz, 2012; Freund and Katona, 2007). In $MEC_{layerII}$, CCKBCs were found to preferentially innervate primarily the non-perforant path forming $calb^+$ principal cells, while avoiding the perforant path forming $reelin^+$ principal cells. Thus, at least certain GABAergic interneurons appeared to be capable of selecting their targets on the basis of long-range projection pattern of principal cells within a single anatomical layer (Varga et al., 2010). At the same time, PV immunolabeling is known to be strong around principal cells in $MEC_{layerII}$ (Wouterlood et al., 1995), and PV immunohisochemistry demonstrated perisomatic contacts around both principal cell populations (Varga et al., 2010). These abundant connections of PV basket cells (PVBCs) with $MEC_{layerII}$ principal cells have been suggested to be important in the formation of grid representations (Couey et al., 2013), and if PVBCs appear to innervate both $calb^+$ and $reelin^+$ populations, it is possible that they exert more influence over the perforant path projection than CCKBCs. The selectivity of heterogeneous GABAergic populations for principal cell subpopulations has been a subject of intense recent interest in other brain regions as well (Lee et al., 2014a; Lee et al., 2014c; for review, see Krook-Magnuson et al., 2012). Interestingly, while CCKBCs in $MEC_{layerII}$ demonstrate a strong preference for $calb^+$ principal cells, they do not appear to be selective

for subpopulations of pyramidal cells defined on the basis of their superficial versus dorsal position within the pyramidal cell layer in the CA1. In contrast, PVBCs in the CA1 provide inhibition preferentially to deep as compared to superficial pyramidal cells, and even within the deep layer, PVBCs are selective with respect to the long-range targets of the pyramidal cells (Lee et al., 2014c). Therefore, in this study we aimed to determine the degree of selectivity that PVBCs in $MEC_{layerII}$ may have with respect to the projection pattern of the postsynaptic target (Fig 1).

Entorhinal Cortex in Epilepsy

There is substantial evidence both from temporal lobe epilepsy (TLE) patients and animal models indicating that the MEC is functionally involved in the development or maintenance of TLE (Bartolomei et al., 2005; Bear et al., 1996; Bragin et al., 2009; Fountain et al., 1998; Gloveli et al., 1998; Heinemann et al., 1993; Jutila et al., 2001; Kobayashi et al., 2003; Pare et al., 1992; Scharfman et al., 1998; Walther et al., 1986). For example, in patients with TLE, spontaneous seizures have been recorded in the entorhinal cortex (Bartolomei et al., 2005; Spencer and Spencer, 1994), and the entorhinal cortex is often smaller in TLE patients (Bernasconi et al., 1999; Jutila et al., 2001). Previous work has demonstrated a decrease in overall gephyrin-labeled punctae (representing inhibitory synapses) throughout the MEC, decreased frequency of spontaneous inhibitory activity in principal cells of the MEC of epileptic animals, and changes in intrinsic properties of principal cells in the region, suggesting a possible role of the MEC in the pathophysiology of TLE in animal models (Hargus et al., 2011; Hargus et al., 2013; Kobayashi et al., 2003; Kumar and Buckmaster, 2006; Kumar et al., 2007). There is also a preferential loss of Layer III pyramidal cells in human patients and animal models (Clifford et al., 1987; Du et al., 1995; Ribak et al., 1998; Schwob et al., 1980; Yilmazer-Hanke et al., 2000), including in the repeated low-dose kainate model (Hellier and Dudek, 2005; Hellier et al., 1998), which we used for these studies.

Because enhanced understanding of the microcircuitry of brain regions can inform the interpretation of changes in epilepsy, in addition to studying PVBC selectivity in juvenile control animals, we also investigated the intrinsic properties and perisomatic inhibitory connectivity of the $MEC_{layerII}$ in older, chronically epileptic and age-matched sham control animals. We focused on perisomatic inhibitory connections with respect to the reelin versus calbindin immunopositivity of their postsynaptic targets within the $MEC_{layerII}$. Specifically, given that PVBCs, in contrast to CCKBCs, seem to provide substantial innervation of $reelin^{+}$ principal cells that form the perforant path, we tested the hypothesis that a selective decrease in PVBC-mediated perisomatic inhibition could explain the apparent hyperexcitability of the input to the hippocampus in epileptic animals (Gloveli et al., 1998; Heinemann et al., 1993; Spencer and Spencer, 1994).

Materials and Methods

Animals

All animal experimentation was conducted in accordance with NIH and UC Irvine IACUC guidelines. Wistar rats were obtained from Charles River. For experiments aimed at

determining the nature of perisomatic PV innervation in $MEC_{layerII}$, 52 juvenile (postnatal day 21–35; 33 male, 19 female) control animals were used. For epilepsy-related studies, older animals were used; a total of 56 female and 50 male epileptic and sham animals were generated at postnatal day 46 using the low-dose kainate model of epilepsy (Hellier et al., 1998). Briefly, animals received 5mg/kg kainate or saline (for sham controls) once per hour until each animal had experienced 3 consecutive hours of stage III–V seizures (on a modified Racine scale). Animals were continuously monitored 3–15 months after epilepsy induction using a telemetric video EEG system (Data Sciences International) and associated Neuroscore software to identify spontaneous seizures at least 3 months after kainate treatment. All epileptic animals were observed to have at least 2 spontaneous stage IV–V seizures during the monitoring period. All animals subjected to the low-dose kainate procedure that were monitored during the study developed epilepsy. None of the sham saline-treated animals had seizures during monitoring. In total, 32 epileptic animals and 23 age-matched sham control animals, aged 46–71 weeks at the time of electrophysiology or immunohistochemistry, were used in the epilepsy-related studies. All epileptic animals were recorded within 1 week of their age-matched sham control. Because of technical difficulty in recording from aged animals, and particularly from epileptic animals, more than one epileptic animal was sometimes recorded at the time of any given age-matched sham control to obtain near equal numbers of data points for all experiments.

Anatomy

Acute horizontal entorhinal-hippocampal slices (60 or 300 μm for immunohistochemistry alone or electrophysiology and post-hoc immunohistochemistry, respectively) were prepared in ice-cold sucrose solution (containing in mM: 85 NaCl, 75 sucrose, 2.5 KCl, 25 glucose, 1.25 NaH_2PO_4, 4 $MgCl_2$, 0.5 $CaCl_2$, 24 $NaHCO_3$), incubated for 1 hour at 32°C, and then stored at room temperature until recording or fixation in 0.1 M phosphate buffer (PB; pH 7.4) containing 4% paraformaldehyde and 0.1% picric acid for 24–48 hours at 4°C. For immunohistochemistry, 60μm horizontal sections were processed with primary antibodies raised against reelin (Millipore, mouse monoclonal antibody, AB5364 clone G10, 1:2,000), calbindin (Swant, rabbit polyclonal antibody D-28k, number CB38, 1:5,000), VGLUT3 (Chemicon, guinea pig polyclonal antibody, AB5421, 1:10,000), PV (Swant, goat polyclonal antibody, number PVG213, 1:1,000), and VGAT (Synaptic Systems, guinea pig polyclonal antibody, number 131 004, 1:1,000), and fluorescent secondary antibodies (Jackson Immunoresearch, Alexa 405 or 594 coupled streptavidin, 405 donkey anti rabbit, 488 donkey anti goat or guinea pig, 594 donkey anti guinea pig, and 649 donkey anti mouse). Primary antibodies were incubated at concentrations specified overnight at 4°C, and were revealed by incubation with secondary antibodies at room temperature for 4 hours. See Table 1 for antibody information and usage. Putative PV boutons were identified by PV and VGAT colocalization and CCK cell boutons were identified using the presynaptic marker VGLUT3 which has been shown to label a subset of CCKBC boutons specifically (Somogyi et al., 2004; Varga et al., 2010). Slices were mounted with Vectashield Antifade Mounting Medium (Vectorlabs H-1000), with age-matched control and epileptic tissue, when applicable, being processed, mounted, and imaged together. Putative boutons were counted from individual frames of 1.2–14.4μm deep z stack confocal images collected randomly from equivalent medial-lateral positions of the middle 1mm of the dorsal-ventral axis of the $MEC_{layerII}$ at

100x with an oil immersion objective using an Olympus Fluoview FV1000 or a Zeiss LSM700 confocal microscope. To ensure equal antibody penetration, for bouton counting experiments, only the outer 15μm of each of the 60μm slices were imaged. Counted single frames in the z direction of the z stack were at least 3μm apart to avoid recounting individual punctae. Boutons surrounding the somata (the perimeter of which was defined by drawing a line tangent to the cell body at the point of apparent dendrite origins and then counting boutons up to the intersection of the dendrite with this tangent line) of all reelin$^+$ and calb$^+$ cells within $MEC_{layerII}$ and fully within the image frame were counted, with the exception of very small cells likely to be interneurons. The perimeter of the membrane used to calculate boutons per mm membrane was established using the length of membrane as calculated by the imaging software used (Axiovision LE, Zeiss) after the perimeter of the cell was outlined by hand by the observer. A single observer evaluated for obvious colocalization in boutons, outlined the cells, and counted all boutons for all experiments by hand. For experiments in juvenile control animals, the observer was blinded to the immunohistochemical identity of the postsynaptic target. For experiments in epileptic and sham animals, the observer was blinded to the epilepsy status of the animal from which slices were taken during counting. For axon tracing experiments, a separate observer performed all counting of putative boutons along the axon. All biocytin-filled axonal enlargements likely to be boutons were counted when the perisomatic contacts appeared to be within 1μm of the somata of calb$^+$ or reelin$^+$ principal cells. For all bouton counting experiments, while electron microscopy was not performed to validate the error rate with selection of boutons, we expect that because all data were analyzed as a comparative study between calb$^+$ and reelin$^+$ cells within individual slices and, when applicable, between epileptic and sham animals in age-matched slices prepared together, the error rate of bouton identification was considered similar for both principal cell populations and between epileptic and age-matched sham control animals.

Electrophysiology

Slices were obtained from juvenile control animals or from adult epileptic or age-matched sham controls, as above aged 21–35 days or 46–71 weeks, respectively. Throughout these experiments, we focused on the middle 1/3 of the MEC in the dorsal ventral axis because inhibitory connectivity and other properties have been shown to vary based on the position of the cells along this axis (Beed et al., 2013; Giocomo et al., 2011; Yoshida et al., 2011). As above, acute horizontal entorhinal-hippocampal slices (300μm) were prepared in ice-cold sucrose solution, incubated for 1 hour at 32°C, and then stored at room temperature until recording. They were then recorded in standard ACSF solution containing (in mM): 126 NaCl, 2.5 KCl, 26 $NaHCO_3$, 2 $CaCl_2$, 2 $MgCl_2$ 1.25 NaH_2PO_4, and 10 glucose. For sIPSC measurements, 5μM NBQX, and 10μM APV were added to the bath. For mIPSC measurements, 1μM TTX was added to the solution used for sIPSC measurements. Slices were visualized under IR-DIC optics, recorded using a MultiClamp 700B amplifier (Molecular Devices, Union City, CA), and Clampex software (version 9.2; Axon Instruments, Burlingame, CA). Whole-cell current clamp recordings were performed with a high Cl^- (33mM) standard internal solution containing (in mM): 90 potassium gluconate, 1.8 NaCl, 1.7 $MgCl_2$, 27.4 KCl, 0.05 EGTA, 10 HEPES, 2 MgATP, 0.4 Na_2GTP, 10 phospho-creatine, and with pH 7.25 at 36°C. All recorded cells were filled with biocytin

added to the internal solution (8mM, Sigma-Aldrich, see Table 1) to allow for post-hoc immunohistochemical and anatomical identification.

Only cells with confirmed profiles were used for analysis of electrophysiology. Confirmation consisted of recovery of the cell for anatomical examination (for interneurons) and colocalization with immunohistochemical markers (including calbindin, reelin, and PV). Clampfit software and MiniAnalysis were used for analysis of electrophysiology. Custom made software for analysis of intrinsic properties was generated in house using MATLAB. Intrinsic properties were examined from a series of negative and positive current steps from the resting membrane potential. Briefly, the following properties were examined by the automated software and are illustrated in Fig 3: **1)** Resting membrane potential (RMP) was defined as the average voltage with 0pA current injection. **2)** Input resistance (R_{in}) was calculated both from the slope of the current/voltage relationship and from the voltage change elicited by the smallest hyperpolarizing and depolarizing current injection steps away from RMP. **3)** Sag amplitude for the most hyperpolarized sweep ($sag_{hyperpol}$) was defined as the difference between the most hyperpolarized point and the steady state voltage of the largest negative current step. **4)** Sag time constant (τ_{sag}) was calculated from the equation of the best fit curve from the most hyperpolarized point of the most hyperpolarized sweep to steady state, defined by $V(t)=V_{max}(1-e^{-t/\tau})$. **5)** Membrane time constant ($\tau_{membrane}$) was calculated both for the time from the current step onset to $1-1/e$ of the peak hyperpolarization, and from the equation of the best fit curve from current step onset to peak hyperpolarization, defined by $V(t)=V_{max}(e^{-t/\tau})$. **6)** Rebound amplitude was defined as the difference between the most depolarized point after the offset of the most hyperpolarized current step and the RMP. **7)** Sag amplitude for the most depolarized sweep without spikes (sag_{depol}) was defined as a sag-like depolarization-induced hyperpolarization which has been observed in stellate cells previously (Alonso and Klink, 1993), and was measured as the amplitude of the most depolarized point after the start of the current injection to the steady state value of the voltage response. **8)** Rheobase was defined as the first current step with spiking activity. In addition, the first regular spiking current injection step was noted, which was the first current step where at least 3 spikes occurred in succession. **9)** Delay to first spike was defined as the time from the current onset to the first spike at the Rheobase. **10)** Interspike interval (ISI) was calculated as the average time between spikes on the least depolarized spiking current step with at least 3 spikes. **11)** Action Potential Threshold (Threshold) was user-selected as described in (Atherton and Bevan, 2005), defined as the point at which the derivative of the voltage trace with respect to time first exceeded the mean over the 50ms prior to the action potential by 2 standard deviations. The thresholds of the first 3 action potentials were averaged to get the value for each cell. **12)** Spike amplitude was measured from threshold to peak of first 3 spikes. **13)** Spike halfwidth was averaged for the first three spikes. **14)** Afterhyperpolarization (AHP) values were calculated as both the immediate fast AHP (fAHP) defined as the first point after which voltage either increases or stabilizes following a spike, the slow AHP (sAHP) which was the most hyperpolarized point between a spike or fAHP if present and the next threshold or the end of the current step. **15)** Depolarizing after potential (DAP) was defined as the most depolarized point between the fAHP and the sAHP, if applicable. Because we noticed that at the most depolarized current sweep, there appeared to be a difference in the first compared to subsequent spikes, we

analyzed the difference in spike properties between the first (denoted by a subscript number 1, e.g. $fAHP_1$) and subsequent 3 spikes on the most depolarized current step recorded (the difference between the first and subsequent spike properties was denoted with a Δ; e.g. ΔfAHP).

Data are presented as mean ± s.e.m., and statistical significance was determined using a two-tailed t-test or a two way ANOVA, with Holm-Sidak post-hoc multiple comparisons test with a level of significance of $p<0.05$. Adjustments for multiple comparisons were made using a Bonferroni correction and the required level of significance on the basis of this correction is reported in each result section, where applicable.

Results

Calbindin containing principal cells receive more spontaneous inhibitory inputs than reelin containing principal cells of $MEC_{layerII}$

Because CCKBCs largely avoid the perforant path forming reelin$^+$ cells, we tested the hypothesis that reelin$^+$ cells would receive fewer inhibitory inputs than calb$^+$ cells. Indeed, the frequency of sIPSCs in reelin$^+$ cells was significantly lower than in calb$^+$ cells (Fig 2a–c; calb$^+$ cell sIPSC frequency 7.7±1.5 Hz, n=19 cells; reelin$^+$ 3.5±1.0 Hz, n=13 cells; n=10 rats; $p<0.05$). The amplitude of events recorded at −80mV in reelin$^+$ cells was not significantly different from events recorded in calb$^+$ cells (calb$^+$ cells amplitude 14.8±0.4 pA; reelin$^+$ cells amplitude 12.6±2.1 pA; $p=0.43$). These findings are consistent with the known preferential innervation of calb$^+$ cells by CCKBCs, and other factors may also contribute to the higher sIPSC frequency in calb$^+$ cells (e.g., preferential innervation of calb$^+$ cells by PVBCs as well, see below).

PVBCs also demonstrate quantitative anatomical selectivity for calbindin-containing principal cells

Given that both reelin$^+$ and calb$^+$ cells receive perisomatic PV inputs while most CCKBC input is onto calb$^+$ cells (Fig 1c, Varga et al., 2010), we tested what, if any, specificity PVBCs might exhibit onto principal cell subpopulations of $MEC_{layerII}$.

We first utilized the colocalization of the presynaptic GABAergic terminal marker, VGAT, with PV to identify putative PV-containing perisomatic boutons by comparing the number of boutons directly surrounding the somata of reelin$^+$ and calb$^+$ principal cells (Fig 2d). Because this was a comparative analysis, the error rate in bouton counting between reelin$^+$ and calb$^+$ cells was considered to be similar.

Interestingly, we found that PVBCs form 38.9% more perisomatic boutons per mm membrane onto calb$^+$ than onto reelin$^+$ cells (Fig 2e; number of PV and VGAT colocalizing punctae per 1 mm of somatic membrane: calb$^+$, 191.4±4.6 punctae per mm membrane, 5818 total punctae, 231 cells; reelin$^+$, 138.8 ±4.9 punctae per mm membrane, 3721 punctae, 192 cells; data collected from 6 juvenile control animals; $p<0.003$). We performed a similar analysis with VGLUT3 (an established marker of CCKBCs Somogyi et al., 2004; Varga et al., 2010) to compare the two perisomatic cell populations, and consistent with prior reports (Varga et al., 2010), we found that CCKBCs formed significantly more boutons onto calb$^+$

than onto reelin$^+$ cells by 196% (Fig 2f; number of VGLUT3 punctae per 1 mm of somatic membrane: calb$^+$, 54.9±2.7 punctae per mm membrane, 880 total punctae, 150 cells; reelin$^+$ 18.6±1.8 punctae per mm membrane, 273 total punctae, 123 cells; data collected from 3 juvenile control animals; $p<0.003$). Additionally, note that there were overall more PV containing boutons per mm membrane than VGLUT3 containing boutons.

Thus, PVBCs also have a quantitative preference for calb$^+$ cells, although they are still less selective of their synaptic targets on the basis of the long-distance axonal projection patterns than CCKBCs, since they do form a sizeable proportion of their axonal contacts with reelin$^+$ as well as calb$^+$ cells.

Intrinsic properties of calbindin and reelin containing principal cells in $MEC_{layerII}$

Within the middle 1mm of the dorsal-ventral axis of the $MEC_{layerII}$, we analyzed the intrinsic properties, including firing patterns, of both reelin$^+$ and calb$^+$ principal cells in juvenile control animals (Fig 3). Descriptions of these measurements are listed in the Materials and methods section and illustrated in Fig 3, and the values are reported in Table 2. After adjusting for multiple comparisons, the intrinsic properties that were significantly different between reelin$^+$ cells (n=15 cells) and calb$^+$ cells (n=21 cells) in the juvenile control animals (n=13 rats) were τ_{sag}, $\tau_{membrane}$, sag_{depol}, rheobase, DAP amplitude, spike $amplitude_1$, $sAHP_1$, DAP_1, ΔfAHP, and ΔsAHP ($p<0.0013$ for each).

In addition, reelin cells did exhibit subthreshold oscillations with average dominant frequency of 7.0±0.4 Hz, similarly to what has been reported in stellate cells previously (Alonso and Klink, 1993; Giocomo et al., 2007). In contrast, calb$^+$ cells demonstrated a dominant oscillation frequency of 5.5±0.2 Hz (compared to reelin$^+$ cells, $p<0.01$). These oscillatory properties were not evaluated further in this study.

Thus, the calb$^+$ and reelin$^+$ principal cell populations had significantly different intrinsic properties, which, as illustrated in the plot in Fig 3f, may allow the separation of the populations on the basis of a multidimensional cluster analysis of their electrophysiological properties.

Individual PVBCs in the $MEC_{layerII}$ form functional connections with both calbindin and reelin containing principal cells

Given that PVBCs form connections with both calb$^+$ and reelin$^+$ principal cell populations, there are two possible, though not mutually exclusive arrangements by which PVBCs could be connected with the two principal cell populations in the $MEC_{layerII}$: either an individual PV cell could innervate both output pathways simultaneously or there could be two separate populations of PVBCs, one of which is selective for reelin$^+$ and one of which is selective for calb$^+$ principal cells (Fig 1b). To begin to evaluate how individual PVBCs are organized with respect to postsynaptic principal cell target, as proof of principle, we traced the individual axons of 5 different biocytin-labeled PVBCs with clear anatomy under fluorescent imaging as they traversed the $MEC_{layerII}$ and counted the number of putative contacts with both calb$^+$ and reelin$^+$ principal cells. We found that all biocytin-filled PVBCs contacted both calb$^+$ and reelin$^+$ cell somata, and that there did not appear to be two separate populations of target-selective PV cells (n=1887 boutons: 1089 onto reelin$^+$, 765 onto calb$^+$,

33 onto double positive cells; 521 total target cells, n=5 filled PV basket cells from 5 different juvenile control animals). However, each individual PV cell varied in terms of the proportion of boutons on calbindin and reelin cells, with extremes being one cell which formed 88% of boutons onto reelin$^+$ and 10% onto calb$^+$ cells, and another cell which formed 19% of boutons onto reelin$^+$ and 80% onto calb$^+$ cells. The boutons of the other three cells were distributed between reelin$^+$ and calb$^+$ cells (specifically, 70%, 63%, 45% onto reelin$^+$ and 29%, 29%, 55% onto calb$^+$ cells, respectively). These were technically difficult experiments requiring extensive axonal biocytin filling and recovery of single filled PV cells, quadruple immunolabeling, and time-intensive imaging. This complexity in this case precluded further processing for electron microscopy to confirm the error rate of putative bouton identification onto both reelin$^+$ and calb$^+$ populations. However, the error rate is expected to be similar between calbindin and reelin cells, and although the methodology may underestimate the number of contacts between PV and reelin$^+$ as compared to calb$^+$ cells, given the more limited cytoplasmic expression of reelin which does not always delimit the membrane location as well as compared to calbindin (for electron microscopic verification of perisomatic inputs to calb$^+$ cells, see Varga et al., 2010), our data qualitatively provide strong support for the presence of boutons onto both reelin$^+$ and calb$^+$ cells from individual PVBCs.

Overall, these data support a range of selectivity amongst individual PVBCs, without a clear bimodal distribution into two selective PVBC populations, and suggest that most PV cells in fact will contact both types of postsynaptic principal cells in $MEC_{layerII}$.

In order to further clarify the issue, as a further proof of principle, we performed paired recordings between PV cells and either postsynaptic calb$^+$ or reelin$^+$ principal cells. The results showed that PVBC-evoked unitary inhibitory postsynaptic currents (uIPSCs) could be recorded with both postsynaptic principal cell populations (onto calb$^+$ cells: n=7; onto reelin$^+$ cells: n=3; pairs recorded from n= 7 juvenile control animals). In fact, in one instance, we were able to record connected pairs from a single PVBC onto both a calb$^+$ cell and a reelin$^+$ cell, confirming that, consistent with the anatomical results described above, a single presynaptic PV cell can indeed form functional connections with both postsynaptic principal cell populations and PVBCs were able to evoke uIPSCs in both reelin$^+$ and calb$^+$ cells.

It is interesting to note that, while exploring the PVBC microcircuitry in the $MEC_{layerII}$ using paired recordings (from n=8 additional juvenile control animals), we also obtained evidence for the existence of synaptic connections between the following cell groups: calb$^+$ principal cells to PVBCs (n=2), PVBCs to $MEC_{layerIII}$ principal cells (n=2), neurogliaform cells (NGFCs) to both calb$^+$ (n=1) and reelin$^+$ (n=2) principal cells, and somatostatin containing (SS) interneurons to both calb$^+$ (n=1) and reelin $^+$ (n=3) principal cells. In 1 additional case, a single presynaptic cell was found to connect to both a calb$^+$ and a reelin$^+$ principal cell (n=1 presynaptic NGFC).

Lack of change in intrinsic properties of principal cell populations in epilepsy

In confirmed spontaneously epileptic and age-matched sham control animals (Fig 4a), we examined whether there were any changes in intrinsic properties in calb$^+$ or reelin$^+$ cells

which might indicate intrinsic hyperexcitability in one or both of the populations of principal cells. We utilized the same methodology and terminology we used in juvenile control animals above (Fig 3) to analyze the intrinsic properties in a blinded fashion. The results are listed in Table 2. The data revealed no significant differences in intrinsic properties between known calb$^+$ and reelin$^+$ cells in adult epileptic (n=8 animals; n=18 reelin$^+$ cells; n=6 calb$^+$ cells) compared to age-matched sham controls (n=6 animals; n=11 reelin$^+$ cells; n=5 calb$^+$ cells) (Table 2; two way ANOVA with p value adjusted for multiple comparisons by Bonferroni correction: $p>0.0015$). Interestingly, however, we did note significant differences between juvenile control animals and recordings from adult animals (numbers as reported above). Specifically, juvenile animals had smaller calb$^+$ fAHP amplitudes, smaller DAP amplitudes in both calb$^+$ and reelin$^+$ cells, and a larger difference in DAP amplitude (ΔDAP) between the first and subsequent three spikes of the most depolarized sweep in reelin$^+$ cells ($p<0.001$ for each), indicating significant alterations in postnatal development from the juvenile stage to adulthood.

Thus, many intrinsic properties remain constant in this model of epilepsy between sham control animals and epileptic animals, although there appear to be significant alterations in intrinsic properties during development from juvenile to adulthood.

Lack of change in perisomatic bouton numbers in epileptic compared to age-matched sham control animals

In slices from 5 video and EEG confirmed epileptic animals (Fig 4a) approximately 12 months post kainate and 4 age-matched sham controls, punctae containing both PV and the presynaptic GABAergic terminal marker, VGAT were counted around calb$^+$ and reelin$^+$ cells using the same technique as for the juvenile control animals described above in connection with Fig 3 (Fig 4b).

Interestingly, there were no differences in the number of punctae surrounding calb$^+$ cells ($p=0.262$), nor surrounding reelin$^+$ cells ($p=0.464$) in epileptic compared to age-matched sham controls (Fig 4c). Specifically, as observed in the juvenile control animals described above, we saw a higher proportion of PV and VGAT containing punctae around calb$^+$ than reelin$^+$ cells in age-matched sham controls (34.4% higher proportion on calb$^+$ cells; number of PV and VGAT colocalizing punctae per 1 mm of somatic membrane: calb$^+$, 158.4±5.5 punctae per mm membrane, 1696 total punctae, 80 cells; reelin$^+$, 117.9 ±7.8 punctae per mm membrane, 1005 punctae, 63 cells; data collected from 4 animals; $p<0.003$). There were also a higher proportion of PV and VGAT positive punctae around calb$^+$ than reelin$^+$ cells in epileptic animals (38.2% higher proportion on calb$^+$ cells; number of PV and VGAT colocalizing punctae per 1 mm of somatic membrane: calb$^+$, 160.2±5.0 punctae per mm membrane, 1449 total punctae, 76 cells; reelin$^+$, 115.9 ±10.5 punctae per mm membrane, 1069 punctae, 68 cells; data collected from 5 animals; $p<0.003$).

To test whether there may have been a selective change in bouton numbers of CCKBCs in epileptic animals, we also examined the number of perisomatic VGLUT3 positive punctae in 3 epileptic and 5 age-matched sham control animals. Surprisingly, there were also no differences in the number of VGLUT3 punctae surrounding calb$^+$ cells ($p=0.561$), nor surrounding reelin$^+$ cells ($p=0.757$) in epileptic compared to age-matched sham controls (Fig

4d). However, as in the young control animals, we still saw a much higher proportion of VGLUT3 positive punctae around calb$^+$ than reelin$^+$ cells in sham controls (400% higher proportion on calb$^+$ cells than reelin cells; number of VGLUT3 punctae per 1 mm of somatic membrane: calb$^+$, 48.6±1.5, 1218 punctae, 325 cells; reelin$^+$, 9.7±0.8 punctae per mm membrane, 316 punctae, 311 cells; data collected from 5 animals; $p<0.003$). There were also a higher proportion of VGLUT3 positive punctae around calb$^+$ than reelin$^+$ cells in epileptic animals (399% higher proportion on calb$^+$ cells; number of VGLUT3 punctae per 1 mm of somatic membrane: calb$^+$, 49.1±3.2 punctae per mm membrane, 293 total punctae, 86 cells; reelin$^+$, 9.8 ±1.6 punctae per mm membrane, 60 punctae, 84 cells; data collected from 3 animals; $p<0.003$).

It should be noted that, despite a lack of difference in the numbers of perisomatic boutons per mm membrane between epileptic and sham controls, we noted that there were significantly fewer VGLUT3 punctae around reelin$^+$ cells in the adult sham controls as compared to juvenile controls described above (9.7±0.8 punctae per 1 mm somatic membrane in adults vs. 18.6±1.8 punctae per 1mm somatic membrane in juvenile controls; $p<0.003$; number of animals and cells as reported above), again (similar to the intrinsic property changes and in PV bouton numbers described above) pointing to developmental alterations during the transition from the juvenile to the adult stage.

To examine whether the lack of difference in PVBC boutons in epileptic animals might be masking a loss of total PV cell numbers combined with a potential axonal sprouting of the surviving cells to generate a similar number of total perisomatic boutons, we counted the total number of PV cells present in 60μm slices from the same epileptic and sham control animals in or immediately adjacent to $MEC_{layerII}$. We observed no change in the number of total PV cells in slices from epileptic animals. Epileptic slices contained 7.1±0.5 PV cells in and immediately adjacent to layer II per slice and control slices contained 6.5±0.5 PV cells per slice (n=57 slices from 7 epileptic animals, n=39 slices from 4 sham control animals; $p=0.52$). This indicates that PV containing cells appear to survive in epilepsy in this model of TLE, and that the number of boutons from each PV cell is likely similar in both sham control and epileptic animals.

Overall, these results showed that the anatomical selectivity of GABAergic perisomatic innervation with respect to postsynaptic principal cell subpopulation appears surprisingly well preserved in $MEC_{layerII}$ in the chronic repeated low dose kainic acid model of epilepsy.

Functional inhibitory events are decreased in epileptic compared to age-matched sham control animals

To examine the overall inhibitory environment for both calb$^+$ and reelin$^+$ cells in $MEC_{layerII}$ in epilepsy, we performed miniature IPSCs (mIPSC) analysis to further evaluate the presynaptic function of the GABAergic synapses onto calb$^+$ and reelin$^+$ cells in epilepsy. Interestingly, although the number of PV and VGLUT3 containing perisomatic boutons was unchanged in epileptic animals for both calb$^+$ and reelin$^+$ cells (see above), there was a significant decrease in the frequency of mIPSCs in all principal cells in epileptic animals compared to age-matched sham controls (Fig 4e; 1.9±0.4 Hz in sham, n= 23 cells from n=3 animals; 1.0±0.1 Hz in epileptic, n= 21 cells from n=3 animals; $p<0.05$). These results

indicate that, despite the lack of anatomical changes in perisomatic bouton numbers, there are presynaptic functional changes in inhibitory input onto principal cells (the nature of these alterations will need to be addressed in future experiments and may include changes in release probability and other changes), consistent with previous studies demonstrating decreased mIPSC frequency in the MEC in the pilocarpine model of epilepsy (Kumar and Buckmaster, 2006).

Direct recurrent excitatory pairs recorded in $MEC_{layerII}$ of epileptic animals

The existence of recurrent excitatory connections in $MEC_{layerII}$ has been investigated using paired recordings, photostimulation, and optogenetics, and suggests that, at best, there is sparse direct excitatory connectivity between principal cells in this layer which decreases dramatically with age, while connections with neighboring cells via excitation of inhibitory cells becomes more common with age (Couey et al., 2013; Dhillon and Jones, 2000; Kumar et al., 2007). In fact, in more than 200 paired recordings in control animals, no clear unitary connections were found between stellate cells (whose electrophysiological properties generally resembled those we observed in reelin$^+$ cells) in adult animals (Couey et al., 2013). In agreement with these results, we observed no excitatory to excitatory cell connections in adult sham control animals (26 tested from 13 stable paired recordings). However, during paired recordings in epileptic animals, we encountered n=3 directly connected pairs between $MEC_{layerII}$ principal cells in 2 epileptic animals older than 450 days (in total, we tested 95 potential connections from 52 stable pairs of principal cells in acute slices from n=6 epileptic animals). Of the connected pairs, 2 pairs were identified with post-hoc immunohistochemistry as being from one reelin$^+$ cell to another reelin$^+$ cell, and 1 pair was from a calb$^+$ cell to a reelin$^+$ cell. During 2 of the 3 paired recordings, NBQX (5μM) and APV (10μM) wash-in abolished the postsynaptic response (Fig 5), and in all 3 pairs, the responses were clearly inward at −20mV postsynaptic holding potential, unlike the recorded uIPSCs described above. This indicates that there may be increased direct recurrent excitatory activity within $MEC_{layerII}$ in epileptic animals that is typically not present in adult animals.

Discussion

While interneuronal diversity has long been recognized as a key factor in determining neuronal network organization, the importance of the relationship between interneuronal diversity and the surprisingly heterogeneous nature of principal cell populations with distinct anatomical and physiological properties and different projection patterns has been only recently recognized (Lee et al., 2014c; Mizuseki et al., 2011; Varga et al., 2010).

Here, we have explored the connectivity of PVBCs in $MEC_{layerII}$ with respect to the subpopulation of the target principal cell, demonstrating that while PVBCs can innervate both perforant-path forming reelin$^+$ and non-perforant path forming calb$^+$ cells simultaneously, they also form more connections with calb$^+$ cells, thus making reelin$^+$ cells much less regulated by perisomatic GABAergic input than would have been previously expected.

In addition, we have also explored the microcircuitry of $MEC_{layerII}$ in the low-dose systemic kainic acid model of TLE with respect to perisomatic input and recurrent connectivity. We found that, surprisingly, at least in this model of chronic TLE in rats, no significant changes occurred in terms of quantitative anatomical connectivity or selectivity either for PVBCs or for CCKBCs. We did find, however, that, in agreement with previous studies (Kumar and Buckmaster, 2006), functional inhibitory connectivity is reduced overall, and we also found direct recurrent unitary connections between $MEC_{layerII}$ principal cells in epileptic animals.

Two populations of principal cells in $MEC_{layerII}$ separated by immunopositivity for calbindin or reelin

We noted again the two distinct populations of pyramidal cells defined by their immunopositivity to $calb^+$ or $reelin^+$ in the $MEC_{layerII}$ (Varga et al., 2010). These subpopulations had significantly different intrinsic properties including subthreshold and spiking features, which might be utilized in future studies to separate the populations on the basis of firing properties rather than solely on immunohistochemical markers. Interestingly, the intrinsic properties of the principal cells in $MEC_{layerII}$ apparently undergo changes during development, which may influence their susceptibility to injury in epilepsy as well.

Previously, the principal cells of $MEC_{layerII}$ have been divided anatomically into stellate cells, pyramidal cells, and cells with tripolar shapes based on axonal and dendritic morphologies (Klink and Alonso, 1997; Pastoll et al., 2012; Ramón y Cajal, 1893). Differences in intrinsic properties have also been reported between the stellate and pyramidal cells as well as within cell types in a dorsal-ventral gradient (Alonso and Klink, 1993; Garden et al., 2008). For example, depolarization-induced early peaking membrane potential during subthreshold depolarizing sweeps (here referred to as sag_{depol}), as well as robust inward-rectification and subthreshold oscillations have been described previously as being unique to stellate cells (Alonso and Klink, 1993; Giocomo et al., 2007). $Reelin^+$ cells in $MEC_{layerII}$ tended to demonstrate these properties, as well as faster sag time constants and prominent oscillation frequencies that were faster than dominant frequencies recorded in $calb^+$ cells. While we did not specifically address the dichotomy of the stellate-pyramidal division with regards to immunohistochemical or electrophysiological identity, the intrinsic properties of the two populations suggest that, at least on average, $reelin^+$ cells comprise primarily stellate cells, whereas $calb^+$ cells comprise primarily pyramidal cells (Alonso and Klink, 1993; Garden et al., 2008; Giocomo et al., 2007; Klink and Alonso, 1997; Pastoll et al., 2012; Ramón y Cajal, 1893).

It is also interesting that in our experiments, we did not observe changes between the intrinsic properties of the distinct subpopulations of principal cells in epileptic versus sham control animals. Instead, we noted differences in intrinsic subthreshold and spiking properties between juvenile and adult animals. Other studies demonstrating changes in intrinsic properties have separated cells on the basis of stellate versus non stellate morphologies rather than $reelin^+$ and $calb^+$ immunohistochemistry, and use different models of epilepsy including the electrical limbic status epilepticus model (Hargus et al., 2011; Hargus et al., 2013), and the pilocarpine model of TLE (Kobayashi et al., 2003; Kumar and Buckmaster, 2006). One possible explanation for our findings is that, given the chronicity of

the epilepsy in the animals from which we recorded the data on intrinsic properties, the cells utilized homeostatic mechanisms through novel conductance combinations that restored near-normal firing properties, as has been shown previously to be possible (Howard et al., 2007; Prinz et al., 2004). These possibilities will need to be addressed with further studies in this model of TLE and looking more specifically at changes in channel expression and individual currents.

Perisomatic GABAergic microcircuitry in juvenile control animals

In juvenile control animals, we found that perisomatic-targeting PVBCs are indeed selective of principal cell type with respect to their divergent outputs from $MEC_{layerII}$, preferentially innervating $calb^+$ principal cells about 40% more than reelin $^+$ cells. Therefore, PVCB-derived inhibition in the MEC is not a homogeneous 'blanket' inhibition as has previously been suggested for neocortical circuits (Packer and Yuste, 2011), similar to findings in the prefrontal cortex and the hippocampus (Lee et al., 2014b; Lee et al., 2014c) but has a preference on the basis of postsynaptic principal cell projection pattern (Krook-Magnuson et al., 2012). However, the PVBC-mediated innervation pattern in the $MEC_{layerII}$ still appears to be much less selective than that of the CCKBCs, which show strong preference for $calb^+$ cells in the $MEC_{layerII}$. Indeed, $reelin^+$ cells appear to receive overall fewer spontaneous events, consistent with their decreased overall inhibitory input from perisomatic GABAergic cells.

However, since PVBCs do still form a significant number of connections with $reelin^+$ cells, the manner in which individual PVBCs interact with their targets was important to elucidate. Rather than finding two subpopulations of PVBC selective for different postsynaptic targets, we found that individual PVBCs do have the capacity to simultaneously influence both perforant path ($reelin^+$) as well as non-perforant path ($calb^+$) output pathways from the $MEC_{layerII}$ using both anatomical axon tracing as well as paired recordings. While we cannot exclude the possibility that additional sub-populations of PV cells may exist that are more selective, both anatomical and electrophysiological data support the ability of most individual PV cells to form functional connections onto both $calb^+$ and $reelin^+$ cells. Further studies will be needed to clarify the degree to which individual PV cells may select their postsynaptic targets on the basis of their immunohistochemical identity and long-distance projection patterns.

It is interesting to consider how the anatomical and functional connectivity of both PV and CCK basket cells may affect the modulation of the output of $MEC_{layerII}$ to separate brain regions in different ways. Generally, CCKBCs, which themselves tend to be more sensitive to a number of types of modulation (Armstrong and Soltesz, 2012), act to preferentially modulate $calb^+$ cells that generate non-perforant path output. At the same time, PVBCs simultaneously modulate both principal cell types, though they, too, have a preference for $calb^+$ cells. Overall, it appears from these data that there is less perisomatic inhibitory control of $reelin^+$ perforant path forming principal cells compared to $calb^+$ principal cells. One interpretation of this finding has to do with the fact that $reelin^+$ cells target the dentate gyrus, where the hyperpolarized resting membrane potentials, relatively high thresholds, and network of strong feed forward and feedback inhibitory inputs to dentate granule cells

contribute to their sparse firing—factors which may have a role in the pattern separation and 'gating' functions of the dentate gyrus (Armstrong et al., 2011; Coulter and Carlson, 2007; de Almeida et al., 2009; Esther et al., 2013; Heinemann et al., 1991; Heinemann et al., 1993; Krook-Magnuson et al., 2015; Leutgeb et al., 2007; Lothman et al., 1991; Mody et al., 1991). Additionally, it could be that the generally strong temporal fidelity of PVBC inputs (Armstrong and Soltesz, 2012) to perforant path forming cells is critical for spatial navigation and memory functions, and other brain regions are perhaps better-suited to also receive inputs modulated by the less temporally precise CCKBCs. An additional layer of complexity is that it is possible that the strong recurrent disynaptic communication between principal cells in $MEC_{layerII}$ through PVBCs (Couey et al., 2013) may contribute to the interplay between principal cells with divergent long-range targets. Understanding the precise relationship between the underlying microcircuitry of $MEC_{layerII}$ will be critical for interpreting the functional implications of microcircuit organization in this region.

Perisomatic inhibitory connections in $MEC_{layerII}$ in epileptic animals in the low-dose kainate model remain anatomically similar in terms of both quantitative contact number and target-selectivity, but mIPSC frequency is reduced

While we had predicted that a decrease in perisomatic inhibition to reelin cells, the principal cells which form the perforant path, might explain the apparent hyperexcitability of input to the dentate gyrus arriving from $MEC_{layerII}$ in epileptic animals (Bear et al., 1996; Bragin et al., 2009; Gloveli et al., 1998; Heinemann et al., 1993; Kobayashi et al., 2003; Kumar and Buckmaster, 2006; Pare et al., 1992; Scharfman et al., 1998; Spencer and Spencer, 1994), interestingly, we found no quantitative difference between the chronically epileptic and age-matched sham control animals in the number of GABAergic PVBC or CCKBC connections to either principal cell population. Because there is evidence from epileptic animals that the number of GABAergic cells and gephyrin-containing punctae (representing GABAergic synapses) are decreased in $MEC_{layerII}$ in epileptic animals (Kumar and Buckmaster, 2006), the lack of change in the number and proportion of both perisomatic PV and VGLUT3 (representing CCK cells) punctae surrounding $calb^+$ and $reelin^+$ somata in $MEC_{layerII}$ is intriguing. This lack of change in bouton numbers does agree well with other evidence that PV containing somata are not lost in $MEC_{layerII}$ of epileptic animals (Drexel et al., 2011), and indeed, we also observed no change in the number of PV cells in epileptic animals. Also, while gephyrin positive punctae were reduced in all layers of the MEC, it is not clear whether changes in layer II might represent reduced inhibition to Layer III pyramidal cells which are frequently lost in epilepsy (Kumar et al., 2007).

However, despite the lack of anatomical changes in perisomatic bouton numbers, there was a decreased mIPSC frequency in $MEC_{layerII}$ principal cells, which is likely to be presynaptic in nature. This suggests that either the existing boutons are not functioning properly (e.g., there is a decrease in the probability of release), or that another population of relatively proximal GABAergic input to these principal cells, the identity of which would remain to be identified, is lost in epilepsy. These findings underscore the need to consider the entire suite of network changes in epilepsy to understand the origins of hyperexcitability in this brain region.

Increased direct recurrent excitatory connections observed between $MEC_{layerII}$ principal cells in adult epileptic animals

The presence of direct excitatory connections in paired recordings between principal cells in adult epileptic animals is interesting. While recurrent axon collaterals of stellate cells can span up to 1mm within $MEC_{layerII}$ and layer I (Lingenhöhl and Finch, 1991), and recurrent excitation was detected by direct photostimulation of layer II principal cells in adult rats in both control and epileptic animals (Kumar et al., 2007), only a few connected paired recordings between principal cells in $MEC_{layerII}$ have ever been achieved, and these were primarily from juvenile animals (in one study, 6 total connected excitatory pairs from 644 total possible pairs were recorded, and all pairs were from animals younger than postnatal day 28) (Couey et al., 2013). In fact, clear direct excitatory paired recordings have not been found between principal cells in $MEC_{layerII}$ of adult animals in acute slices to date (Couey et al., 2013; Dhillon and Jones, 2000), and in contrast to the photostimulation experiments described above, direct optogenetic stimulation of $MEC_{layerII}$ principal cells did not reveal direct recurrent excitatory connections (Couey et al., 2013). Thus, our data suggest that there may be an increased probability of local recurrent excitatory connectivity in this model of epilepsy, in at least some animals, that can be probed using paired recordings. Additional experiments will be needed to understand how recurrent excitatory connectivity may change in this region in epilepsy.

Conclusions and Outlook

The results presented in this study help to elucidate both the normal and pathological roles of major perisomatic GABAergic cell types in the $MEC_{layerII}$ with reference to the immunohistochemical profiles of the postsynaptic targets, which are known to relate to the long-range targets of principal cells in this region (Ray et al., 2014; Varga et al., 2010). Future studies will be necessary to better understand how $MEC_{layerII}$ is organized in terms of interneuronal target specificity and its relationship to principal cell subtypes, and how this organization may change in epilepsy. For example, future projects may identify the mechanisms by which $calb^{+}$ cells might selectively recruit perisomatic GABAergic inputs, determine how perforant path and non-perforant path projecting cells may respond differently to coregulation by common PV inputs, elucidate the connectivity patterns of other types of interneurons in the region with respect to postsynaptic principal cell targets, understand the connection between cell type and functional role in terms of spatial navigation, and reveal the cell-type specificity of changes seen in this region in epileptic animals. Such studies will help unravel the role of the divergence in perisomatic inhibition to subpopulations of postsynaptic targets in normal functions of entorhinal-hippocampal connections such as spatial navigation and memory, and in addition will allow better understanding of the functional and cognitive implications of the pathological changes that are seen in the region in temporal lobe epilepsy.

Acknowledgments

Grant sponsor: NIH; Grant number: R01 NS74432.

We would like to thank all members of the Soltesz lab, especially Csaba Varga for his tutelage and essential advice in troubleshooting of immunohistochemistry, anatomy, and confocal microscopy; Kevin Ding, Rose Zhu and Judit

Vargane for technical support; Laura Ewell, Ronald Seese, and Courtney Burgdorff for valuable conversations and morale; and Marcella Evans for assistance with preliminary experiments. We thank Steven Ross for the loan of the Nikon FN-1 Eclipse microscope, and the confocal facility of the Optical Biology Shared Resource of the Cancer Center Support Grant (CA-62203) at the University of California, Irvine. This work was supported financially by the UCI MSTP (to CA), the NSF (NSF DGE-0808392 to MB), & the NIH (R01 NS74432 to IS).

References

Alonso A, Klink R. Differential electroresponsiveness of stellate and pyramidal-like cells of medial entorhinal cortex layer II. Journal of Neurophysiology. 1993; 70(1):128–143. [PubMed: 8395571]

Armstrong C, Soltesz I. Basket cell dichotomy in microcircuit function. The Journal of Physiology. 2012; 590(Pt 4):683–694. [PubMed: 22199164]

Armstrong C, Szabadics J, Tamas G, Soltesz I. Neurogliaform cells in the molecular layer of the dentate gyrus as feed-forward gamma-aminobutyric acidergic modulators of entorhinal-hippocampal interplay. J Comp Neurol. 2011; 519(8):1476–91. [PubMed: 21452204]

Atherton JF, Bevan MD. Ionic mechanisms underlying autonomous action potential generation in the somata and dendrites of GABAergic substantia nigra pars reticulata neurons in vitro. The Journal of Neuroscience. 2005; 25(36):8272–8281. [PubMed: 16148235]

Bartolomei F, Khalil M, Wendling F, Sontheimer A, Regis J, Ranjeva JP, Guye M, Chauvel P. Entorhinal cortex involvement in human mesial temporal lobe epilepsy: an electrophysiologic and volumetric study. Epilepsia. 2005; 46(5):677–87. [PubMed: 15857433]

Bear J, Fountain NB, Lothman EW. Responses of the superficial entorhinal cortex in vitro in slices from naive and chronically epileptic rats. J Neurophysiol. 1996; 76(5):2928–40. [PubMed: 8930245]

Beed P, Gundlfinger A, Schneiderbauer S, Song J, Böhm C, Burgalossi A, Brecht M, Vida I, Schmitz D. Inhibitory gradient along the dorsoventral axis in the medial entorhinal cortex. Neuron. 2013; 79(6):1197–1207. [PubMed: 24050405]

Bernasconi N, Bernasconi A, Andermann F, Dubeau F, Feindel W, Reutens DC. Entorhinal cortex in temporal lobe epilepsy: a quantitative MRI study. Neurology. 1999; 52(9):1870–6. [PubMed: 10371536]

Bragin DE, Sanderson JL, Peterson S, Connor JA, Muller WS. Development of epileptiform excitability in the deep entorhinal cortex after status epilepticus. Eur J Neurosci. 2009; 30(4):611–24. [PubMed: 19674083]

Chin J, Massaro CM, Palop JJ, Thwin MT, Yu G-Q, Bien-Ly N, Bender A, Mucke L. Reelin depletion in the entorhinal cortex of human amyloid precursor protein transgenic mice and humans with Alzheimer's disease. The Journal of Neuroscience. 2007; 27(11):2727–2733. [PubMed: 17360894]

Clifford DB, Olney JW, Maniotis A, Collins RC, Zorumski CF. The functional anatomy and pathology of lithium-pilocarpine and high-dose pilocarpine seizures. Neuroscience. 1987; 23(3):953–68. [PubMed: 3437996]

Couey JJ, Witoelar A, Zhang S-J, Zheng K, Ye J, Dunn B, Czajkowski R, Moser M-B, Moser EI, Roudi Y, et al. Recurrent inhibitory circuitry as a mechanism for grid formation. Nat Neurosci. 2013; 16(3):318–324. [PubMed: 23334580]

Coulter DA, Carlson GC. Functional regulation of the dentate gyrus by GABA-mediated inhibition. Progress in brain research. 2007; 163:235–812. [PubMed: 17765722]

de Almeida L, Idiart M, Lisman JE. The input–output transformation of the hippocampal granule cells: from grid cells to place fields. The Journal of Neuroscience. 2009; 29(23):7504–7512. [PubMed: 19515918]

Deng PY. GABAB Receptor Activation Inhibits Neuronal Excitability and Spatial Learning in the Entorhinal Cortex by Activating TREK-2 K+ Channels. 2009; 63:230–243.

Dhillon A, Jones RS. Laminar differences in recurrent excitatory transmission in the rat entorhinal cortex in vitro. Neuroscience. 2000; 99(3):413–422. [PubMed: 11029534]

Drexel M, Preidt AP, Kirchmair E, Sperk G. Parvalbumin interneurons and calretinin fibers arising from the thalamic nucleus reuniens degenerate in the subiculum after kainic acid-induced seizures. Neuroscience. 2011; 189:316–29. [PubMed: 21616128]

Du F, Eid T, Lothman EW, Kohler C, Schwarcz R. Preferential neuronal loss in layer III of the medial entorhinal cortex in rat models of temporal lobe epilepsy. J Neurosci. 1995; 15(10):6301–13. [PubMed: 7472396]

Esther PY, Dengler CG, Frausto SF, Putt ME, Yue C, Takano H, Coulter DA. Protracted postnatal development of sparse, specific dentate granule cell activation in the mouse hippocampus. The Journal of Neuroscience. 2013; 33(7):2947–2960. [PubMed: 23407953]

Fountain NB, Bear J, Bertram EH 3rd, Lothman EW. Responses of deep entorhinal cortex are epileptiform in an electrogenic rat model of chronic temporal lobe epilepsy. J Neurophysiol. 1998; 80(1):230–40. [PubMed: 9658044]

Freund TF, Katona I. Perisomatic inhibition. Neuron. 2007; 56(1):33–42. [PubMed: 17920013]

Fujimaru Y, Kosaka T. The distribution of two calcium binding proteins, calbindin D-28K and parvalbumin, in the entorhinal cortex of the adult mouse. 1996; 24:329–343.

Garden DL, Dodson PD, O'Donnell C, White MD, Nolan MF. Tuning of synaptic integration in the medial entorhinal cortex to the organization of grid cell firing fields. Neuron. 2008; 60(5):875–889. [PubMed: 19081381]

Giocomo LM, Hussaini SA, Zheng F, Kandel ER, Moser MB, Moser EI. Grid cells use HCN1 channels for spatial scaling. Cell. 2011; 147(5):1159–70. [PubMed: 22100643]

Giocomo LM, Zilli EA, Fransén E, Hasselmo ME. Temporal frequency of subthreshold oscillations scales with entorhinal grid cell field spacing. Science. 2007; 315(5819):1719–1722. [PubMed: 17379810]

Gloveli T, Schmitz D, Heinemann U. Interaction between superficial layers of the entorhinal cortex and the hippocampus in normal and epileptic temporal lobe. Epilepsy Res. 1998; 32(1–2):183–93. [PubMed: 9761319]

Hafting T, Fyhn M, Molden S, Moser MB, Moser EI. Microstructure of a spatial map in the entorhinal cortex. 2005; 436:801–806.

Hargus NJ, Merrick EC, Nigam A, Kalmar CL, Baheti AR, Bertram EH, Patel MK. Temporal lobe epilepsy induces intrinsic alterations in Na channel gating in layer II medial entorhinal cortex neurons. Neurobiology of disease. 2011; 41(2):361–376. [PubMed: 20946956]

Hargus NJ, Nigam A, Bertram EH, Patel MK. Evidence for a role of Na(v)1.6 in facilitating increases in neuronal hyperexcitability during epileptogenesis. Journal of Neurophysiology. 2013; 110(5): 1144–1157. [PubMed: 23741036]

Heinemann U, Beck H, Dreier J, Ficker E, Stabel J, Zhang C. The dentate gyrus as a regulated gate for the propagation of epileptiform activity. Epilepsy research Supplement. 1991; 7:273–280. [PubMed: 1334666]

Heinemann U, Zhang CL, Eder C. Entorhinal cortex-hippocampal interactions in normal and epileptic temporal lobe. Hippocampus. 1993; 3(Spec No):89–97. [PubMed: 8287114]

Hellier JL, Dudek FE. Chemoconvulsant model of chronic spontaneous seizures. Curr Protoc Neurosci. 2005; Chapter 9(Unit 9):19. [PubMed: 18428628]

Hellier JL, Patrylo PR, Buckmaster PS, Dudek FE. Recurrent spontaneous motor seizures after repeated low-dose systemic treatment with kainate: assessment of a rat model of temporal lobe epilepsy. Epilepsy Res. 1998; 31(1):73–84. [PubMed: 9696302]

Howard AL, Neu A, Morgan RJ, Echegoyen JC, Soltesz I. Opposing Modifications in Intrinsic Currents and Synaptic Inputs in Post-Traumatic Mossy Cells: Evidence for Single-Cell Homeostasis in a Hyperexcitable Network. Journal of Neurophysiology. 2007; 97(3):2394–2409. [PubMed: 16943315]

Jutila L, Ylinen A, Partanen K, Alafuzoff I, Mervaala E, Partanen J, Vapalahti M, Vainio P, Pitkanen A. MR volumetry of the entorhinal, perirhinal, and temporopolar cortices in drug-refractory temporal lobe epilepsy. AJNR Am J Neuroradiol. 2001; 22(8):1490–501. [PubMed: 11559496]

Kitamura T, Pignatelli M, Suh J, Kohara K, Yoshiki A, Abe K, Tonegawa S. Island cells control temporal association memory. Science. 2014; 343(6173):896–901. [PubMed: 24457215]

Klink R, Alonso A. Morphological characteristics of layer II projection neurons in the rat medial entorhinal cortex. Hippocampus. 1997; 7(5):571–583. [PubMed: 9347353]

Kobayashi M, Wen X, Buckmaster PS. Reduced inhibition and increased output of layer II neurons in the medial entorhinal cortex in a model of temporal lobe epilepsy. J Neurosci. 2003; 23(24):8471–9. [PubMed: 13679415]

Kohara K, Pignatelli M, Rivest AJ, Jung H-Y, Kitamura T, Suh J, Frank D, Kajikawa K, Mise N, Obata Y. Cell type-specific genetic and optogenetic tools reveal hippocampal CA2 circuits. Nature neuroscience. 2014; 17(2):269–279. [PubMed: 24336151]

Krook-Magnuson E, Varga C, Lee S-H, Soltesz I. New dimensions of interneuronal specialization unmasked by principal cell heterogeneity. Trends in Neurosciences. 2012; 35(3):175–184. [PubMed: 22119146]

Krook-Magnuson E, Armstrong C, Bui A, Lew S, Oijala M, Soltesz I. In vivo evaluation of the dentate gate theory in epilepsy. The Journal of Physiology. 2015

Kumar SS, Buckmaster PS. Hyperexcitability, interneurons, and loss of GABAergic synapses in entorhinal cortex in a model of temporal lobe epilepsy. J Neurosci. 2006; 26(17):4613–23. [PubMed: 16641241]

Kumar SS, Jin X, Buckmaster PS, Huguenard JR. Recurrent Circuits in Layer II of Medial Entorhinal Cortex in a Model of Temporal Lobe Epilepsy. The Journal of Neuroscience. 2007; 27(6):1239–1246. [PubMed: 17287497]

Lee AT, Gee SM, Vogt D, Patel T, Rubenstein JL, Sohal VS. Pyramidal neurons in prefrontal cortex receive subtype-specific forms of excitation and inhibition. Neuron. 2014a; 81(1):61–8. [PubMed: 24361076]

Lee AT, Vogt D, Rubenstein JL, Sohal VS. A class of GABAergic neurons in the prefrontal cortex sends long-range projections to the nucleus accumbens and elicits acute avoidance behavior. J Neurosci. 2014b; 34(35):11519–25. [PubMed: 25164650]

Lee S-H, Marchionni I, Bezaire M, Varga C, Danielson N, Lovett-Barron M, Losonczy A, Soltesz I. Parvalbumin-Positive Basket Cells Differentiate among Hippocampal Pyramidal Cells. Neuron. 2014c; 82(5):1129–1144. [PubMed: 24836505]

Leutgeb JK, Leutgeb S, Moser M-B, Moser EI. Pattern separation in the dentate gyrus and CA3 of the hippocampus. science. 2007; 315(5814):961–966. [PubMed: 17303747]

Lingenhöhl K, Finch D. Morphological characterization of rat entorhinal neurons in vivo: soma-dendritic structure and axonal domains. Experimental brain research. 1991; 84(1):57–74. [PubMed: 1713171]

Lothman E, Stringer J, Bertram E. The dentate gyrus as a control point for seizures in the hippocampus and beyond. Epilepsy research Supplement. 1991; 7:301–313. [PubMed: 1334669]

Mizuseki K, Diba K, Pastalkova E, Buzsaki G. Hippocampal CA1 pyramidal cells form functionally distinct sublayers. Nat Neurosci. 2011; 14(9):1174–81. [PubMed: 21822270]

Mizuseki K, Sirota A, Pastalkova E, Buzsaki G. Theta Oscillations Provide Temporal Windows for Local Circuit Computation in the Entorhinal-Hippocampal Loop. 2009; 64:267–280.

Mody I, Köhr G, Otis TS, Staley K. The electrophysiology of dentate gyrus granule cells in whole-cell recordings. Epilepsy research Supplement. 1991; 7:159–168. [PubMed: 1334661]

Packer AM, Yuste R. Dense, Unspecific Connectivity of Neocortical Parvalbumin-Positive Interneurons: A Canonical Microcircuit for Inhibition? The Journal of Neuroscience. 2011; 31(37):13260–13271. [PubMed: 21917809]

Pare D, deCurtis M, Llinas R. Role of the hippocampal-entorhinal loop in temporal lobe epilepsy: extra- and intracellular study in the isolated guinea pig brain in vitro. J Neurosci. 1992; 12(5):1867–81. [PubMed: 1578275]

Pastoll H, Ramsden H, Nolan MF. Intrinsic electrophysiological properties of entorhinal cortex stellate cells and their contribution to grid cell firing fields. Frontiers in Neural Circuits. 2012:6. [PubMed: 22363267]

Prinz AA, Bucher D, Marder E. Similar network activity from disparate circuit parameters. Nat Neurosci. 2004; 7(12):1345–1352. [PubMed: 15558066]

Ramón y Cajal S. Estructura del asta de ammon y fascia dentata: tip. de Fortanet. 1893

Ramos-Moreno T, Galazo MJ, Porrero C, Martínez-Cerdeño V, Clascá F. Extracellular matrix molecules and synaptic plasticity: immunomapping of intracellular and secreted Reelin in the adult rat brain. European Journal of Neuroscience. 2006; 23(2):401–422. [PubMed: 16420448]

Ray S, Naumann R, Burgalossi A, Tang Q, Schmidt H, Brecht M. Grid-layout and theta-modulation of layer 2 pyramidal neurons in medial entorhinal cortex. Science. 2014; 343(6173):891–896. [PubMed: 24457213]

Ribak CE, Seress L, Weber P, Epstein CM, Henry TR, Bakay RA. Alumina gel injections into the temporal lobe of rhesus monkeys cause complex partial seizures and morphological changes found in human temporal lobe epilepsy. J Comp Neurol. 1998; 401(2):266–90. [PubMed: 9822153]

Rowland DC, Weible AP, Wickersham IR, Wu H, Mayford M, Witter MP, Kentros CG. Transgenically targeted rabies virus demonstrates a major monosynaptic projection from hippocampal area CA2 to medial entorhinal layer II neurons. The Journal of Neuroscience. 2013; 33(37):14889–14898. [PubMed: 24027288]

Scharfman HE, Goodman JH, Du F, Schwarcz R. Chronic changes in synaptic responses of entorhinal and hippocampal neurons after amino-oxyacetic acid (AOAA)-induced entorhinal cortical neuron loss. J Neurophysiol. 1998; 80(6):3031–46. [PubMed: 9862904]

Schwob JE, Fuller T, Price JL, Olney JW. Widespread patterns of neuronal damage following systemic or intracerebral injections of kainic acid: a histological study. Neuroscience. 1980; 5(6):991–1014. [PubMed: 7402461]

Solstad T, Boccara CN, Kropff E, Moser MB, Moser EI. Representation of Geometric Borders in the Entorhinal Cortex. 2008; 322:1865–1868.

Somogyi J, Baude A, Omori Y, Shimizu H, Mestikawy SE, Fukaya M, Shigemoto R, Watanabe M, Somogyi P. GABAergic basket cells expressing cholecystokinin contain vesicular glutamate transporter type 3 (VGLUT3) in their synaptic terminals in hippocampus and isocortex of the rat. European Journal of Neuroscience. 2004; 19(3):552–569. [PubMed: 14984406]

Spencer SS, Spencer DD. Entorhinal-hippocampal interactions in medial temporal lobe epilepsy. Epilepsia. 1994; 35(4):721–7. [PubMed: 8082614]

Steward O. Topographic organization of the projections from the entorhinal area to the hippocampal formation of the rat. J Comp Neurol. 1976; 167(3):285–314. [PubMed: 1270625]

Steward O, Scoville SA. Cells of origin of entorhinal cortical afferents to the hippocampus and fascia dentata of the rat. Journal of Comparative Neurology. 1976; 169(3):347–370. [PubMed: 972204]

van Strien NM, Cappaert NL, Witter MP. The anatomy of memory: an interactive overview of the parahippocampal-hippocampal network. Nat Rev Neurosci. 2009; 10(4):272–82. [PubMed: 19300446]

Varga C, Lee SY, Soltesz I. Target-selective GABAergic control of entorhinal cortex output. Nat Neurosci. 2010; 13(7):822–4. [PubMed: 20512133]

Walther H, Lambert JD, Jones RS, Heinemann U, Hamon B. Epileptiform activity in combined slices of the hippocampus, subiculum and entorhinal cortex during perfusion with low magnesium medium. Neurosci Lett. 1986; 69(2):156–61. [PubMed: 3763042]

Wouterlood F, Härtig W, Brückner G, Witter M. Parvalbumin-immunoreactive neurons in the entorhinal cortex of the rat: localization, morphology, connectivity and ultrastructure. Journal of Neurocytology. 1995; 24(2):135–153. [PubMed: 7745443]

Yilmazer-Hanke DM, Wolf HK, Schramm J, Elger CE, Wiestler OD, Blumcke I. Subregional pathology of the amygdala complex and entorhinal region in surgical specimens from patients with pharmacoresistant temporal lobe epilepsy. J Neuropathol Exp Neurol. 2000; 59(10):907–20. [PubMed: 11079781]

Yoshida M, Giocomo LM, Boardman I, Hasselmo ME. Frequency of subthreshold oscillations at different membrane potential voltages in neurons at different anatomical positions on the dorsoventral axis in the rat medial entorhinal cortex. The Journal of Neuroscience. 2011; 31(35): 12683–12694. [PubMed: 21880929]

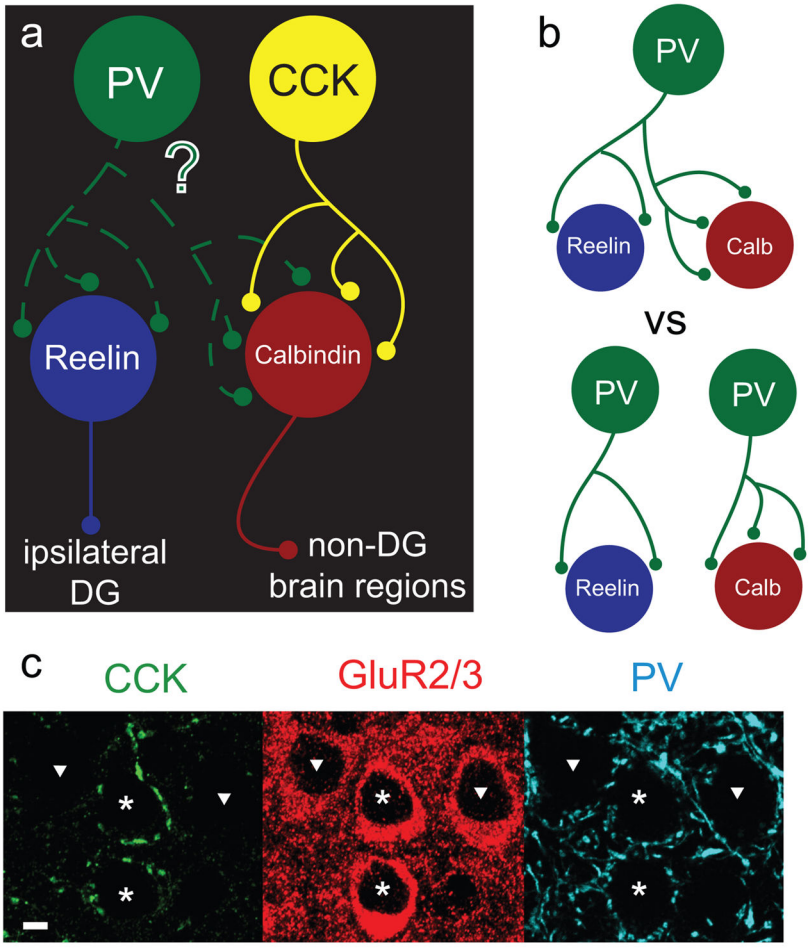

Figure 1. Schematic of experimental question

a.) Perisomatically-targeting CCK positive basket cells (CCKBCs) selectively target non-perforant path forming calbindin positive (calb$^+$) principal cells while largely avoiding ipsilaterally-projecting reelin positive (reelin$^+$) principal cells that form the perforant path (DG= dentate gyrus). We investigate in this study whether PV containing basket cells (PVBCs) select their targets with respect to long-range projection pattern. b) Since PVBCs do contact both types of principal cell (Varga et al., 2010), it is possible that individual PVBCs are either simultaneously contacting both calb$^+$ and reelin$^+$ principal cells (top), or that there are two subpopulations of PVBCs that are each selective for one principal cell type (bottom). c) This image was reproduced with permission from Varga et al., 2010 Nature Neuroscience, and demonstrates that CCK-immunopositive axon terminals (left panel) selectively surround the somata of some (asterisks) but not all (triangles) principal cells in $MEC_{layerII}$ (principal cells were visualized by GluR2/3 immunopositivity; middle panel). In contrast, axons from PVBCs (right panel) surround the perisomatic region of most principal cells. Scale bar in c = 10μm.

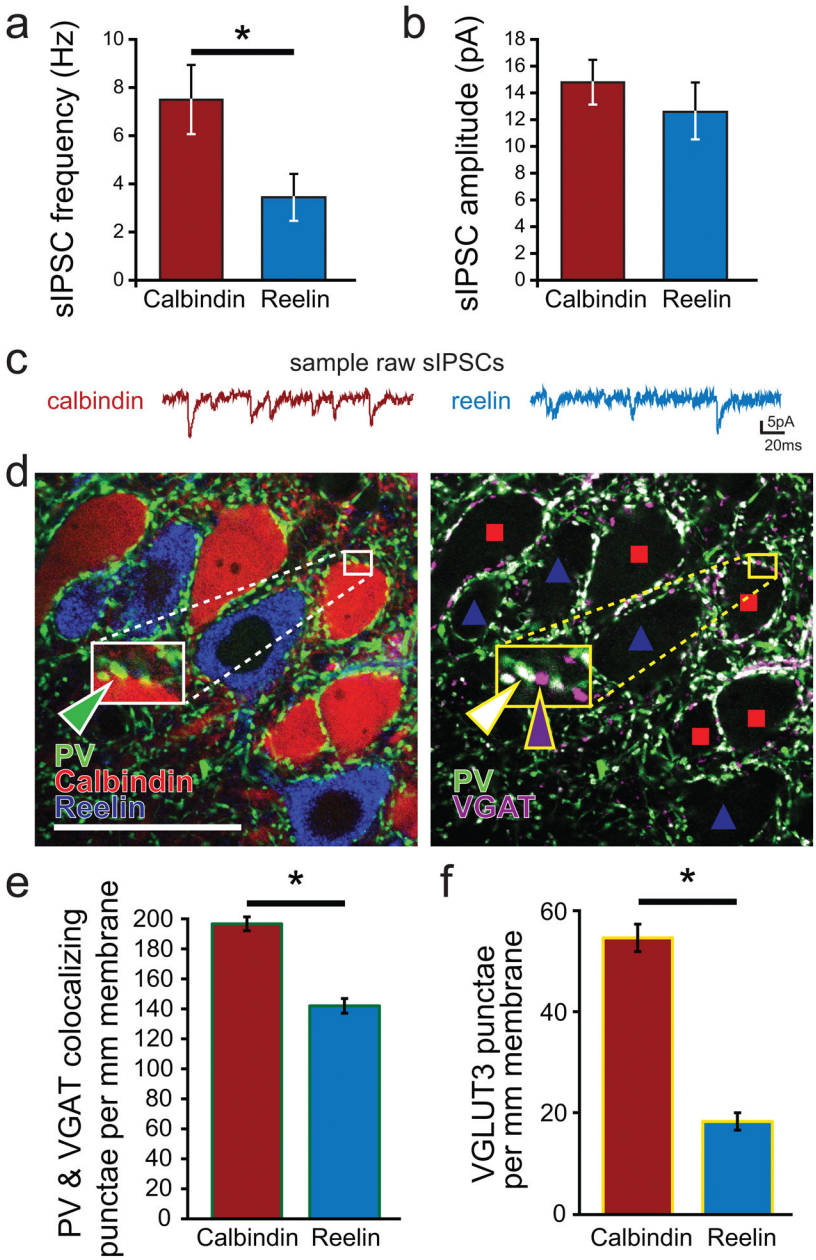

Figure 2. Functional and anatomical differences in GABAergic inputs to principal cells in $MEC_{layerII}$

a) Frequency and b) amplitude of spontaneous inhibitory postsynaptic currents (sIPSCs) recorded from calbindin positive ($calb^+$) and reelin positive ($reelin^+$) principal cells. Consistent with the reduced anatomical presence of perisomatic GABAergic contacts, $reelin^+$ cells also had a lower sIPSC frequency. c) Example raw traces of sIPSC measurements recorded in $calb^+$ (left) and $reelin^+$ (right) cells. d) An example of the immunohistochemical markers (note that colorization of fluorescent channels has been optimized for clarity between different experiments and does not represent the fluorophore used for visualization) calbindin (red), reelin (blue), PV (green), and VGAT (magenta). When PV (shown in green with reelin and calbindin on the left panel) is combined with

VGAT immunohistochemistry to identify presynaptic GABAergic terminals (image shown on right demonstrating PV in green and VGAT in magenta, with locations of calb$^+$ and reelin$^+$ cells denoted by red squares and blue triangles, respectively), synaptic regions can be identified by colocalization, shown in white. Insets: Note that calb$^+$ cells receive both individual PV boutons (green triangle on left panel; shown colocalizing with VGAT, white triangle, on right panel) as well as numerous VGAT positive punctae without PV (magenta arrow) (which may represent CCKBC terminals, because only two types of basket cells provide innervation to principal cells in cortical circuits, the CCKBCs and the PVBCs), while reelin$^+$ cells have few such punctae (scale bar = 50μm). e) More PV containing punctae surround the somata of calb$^+$ than reelin$^+$ principal cells. e) CCKBCs, whose punctae can be identified by the marker VGLUT3, were again seen to have a strong preference for calb$^+$ as compared to reelin$^+$ cells in juvenile animals.

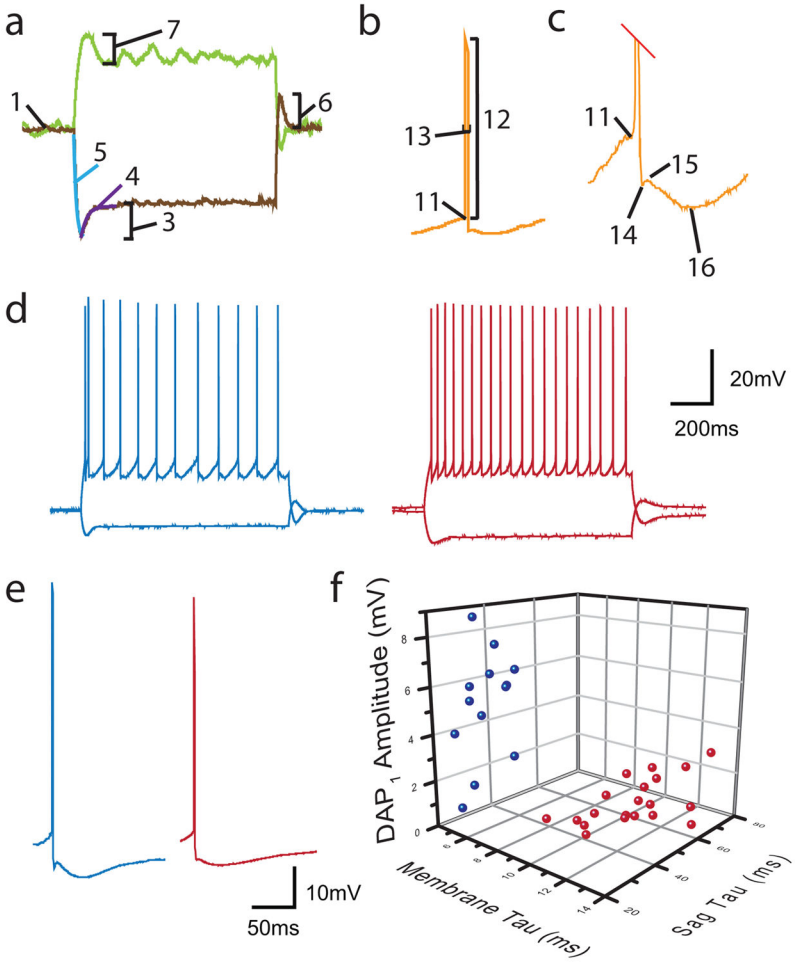

Figure 3. Intrinsic properties of calbindin and reelin cells and paired recording between a single PV basket cells and a postsynaptic calbindin and a reelin principal cell in MEC $_{\text{layerII}}$

Properties measured include (see Materials and methods section for detailed descriptions): a) hyperpolarizing and depolarizing subthreshold sweeps demonstrating the 1) RMP, 2) R_{in} (not shown), 3) $sag_{hyperpol}$, 4) τ_{sag}, 5) $\tau_{membrane}$, 6) rebound amplitude, 7) sag_{depol} First spiking trace not shown includes: 8) rheobase (first sweep with spikes, not shown), 9) delay to first spike (not shown), 10) ISI (not shown), b) A single spike with labels for: 11) threshold, 12) spike amplitude, 13) spike halfwidth, c) Trace in (b) zoomed in on the AHP region of the spike to demonstrate: 14) fAHP 15) DAP 16) sAHP. d) Firing patterns of reelin (left, blue) and calbindin (right, red) containing principal cells differed in a number of ways; pictured are examples of regular spiking sweeps from both cell types and e) examples of the first spike from the first spiking depolarizing sweep from reelin (left, blue) and calbindin (right, red) cells. f) Example 3-dimensional plot of three different measured intrinsic properties that differed significantly between all calbindin (red dots) and reelin (blue dots) cells demonstrates clear separation of calbindin and reelin containing cell populations.

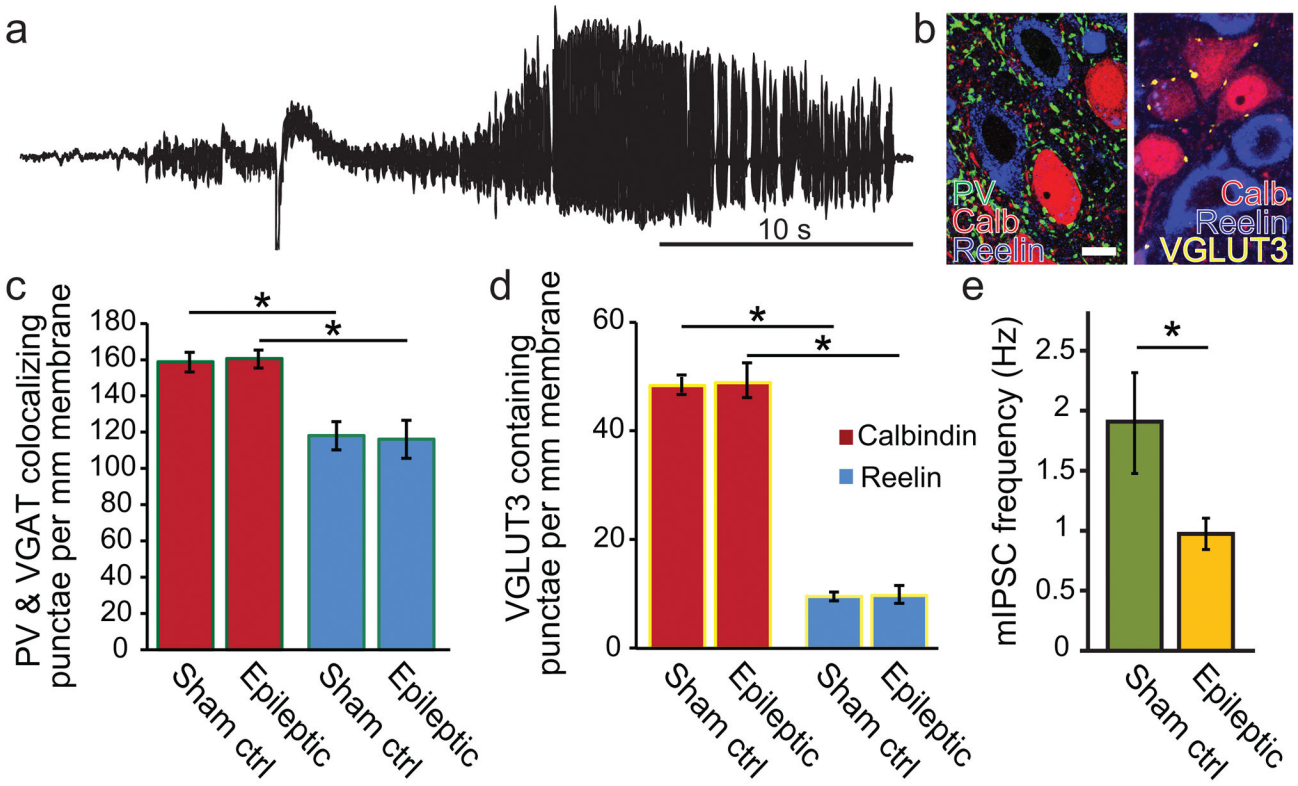

Figure 4. Anatomical and functional GABAergic connections in principal cells of $MEC_{layerII}$ of epileptic animals

Epileptic animals were generated using the low dose kainate model and monitored for spontaneous recurrent seizures using continuous video and EEG monitoring. a) An example of a spontaneous behavioral and electrographic seizure recorded in a chronically epileptic rat used for this study. b) An example of the immunohistochemical markers in tissue from epileptic animals (note that colorization of fluorescent channels has been optimized for clarity between different experiments and does not represent the fluorophore used for visualization): calbindin (red), reelin (blue), PV (green), and VGLUT3 (yellow). Left panel shows PV, calbindin, and reelin only, while right panel shows VGLUT3, calbindin, and reelin only. (scale bar = 10μm). c) In both age-matched sham controls and chronically epileptic animals, PV basket cells (PVBCs) preferentially formed perisomatic punctae around calbindin ($calb^+$) containing compared to reelin ($reelin^+$) containing principal cells, and d) VGLUT3 positive perisomatic punctae had a strong quantitative preference for $calb^+$ compared to $reelin^+$ cells, which did not differ in epileptic animals. e) Miniature inhibitory postsynaptic currents (mIPSCs) were reduced in epileptic compared to age-matched sham controls.

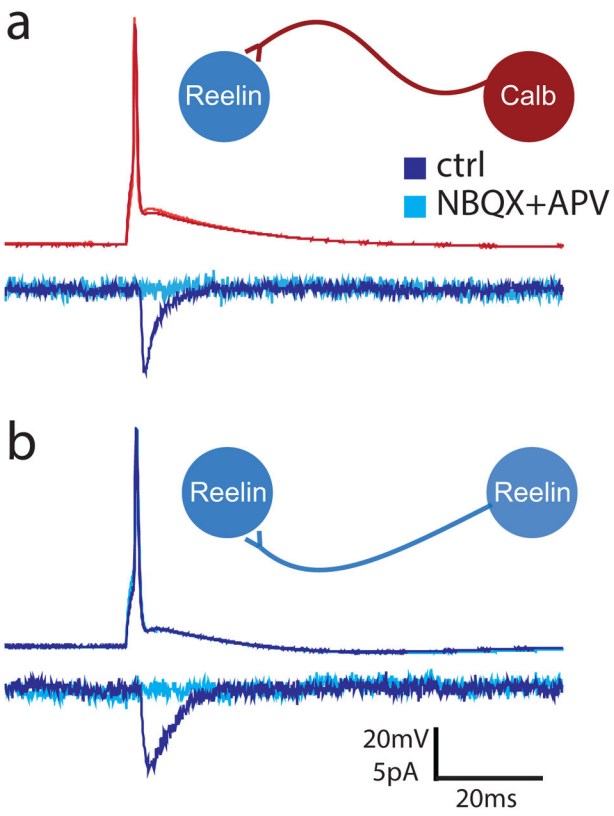

Figure 5. Example unitary excitatory pair recordings between immunohistochemically identified $MEC_{layerII}$ principal cells in epileptic animals

a) An example of a direct excitatory connection recorded from a calbindin ($calb^+$) to a reelin ($reelin^+$) containing principal cell in an epileptic animal (inset). b) Another example pair, this time between two $reelin^+$ cells (inset). For both panels: recordings performed in a K-gluconate based solution. Upper traces show the presynaptic spike, lower traces demonstrate the response in the postsynaptic cell in ACSF (dark blue, dark red) that was abolished in AMPA/kainate and NMDA antagonists, NBQX and APV (light blue, light red).

Table 1

Antibodies and other reagents used for cell detection and associated catalogue information

See methods and results for descriptions of use. Immunogen detected is listed on the leftmost column, along with the primary and secondary antibodies used in specified experiments and concentrations. Manufacturer information contains hyperlinks to websites for the products used in these experiments.

detection of:	experiments	antibody	antibody	manufacturer & catalogue number	concentration
reelin	all	primary	mouse anti-reelin	Millipore monoclonal AB5364 clone G10	1:2,000
		secondary	Alexa 647 donkey anti-mouse	Jackson Immunoresearch 715-605-151	1:500
calbindin	all except PV axon tracing	primary	rabbit anti-calbindin	Swant polyclonal antibody D-28k, number CB38	1:5,000
		secondary	Alexa 594 donkey anti-rabbit	Jackson Immunoresearch 711-585-152	1:500
calbindin	PV cell axon tracing only	primary	rabbit anti-calbindin	Swant polyclonal antibody D-28k, number CB38	1:5,000
		secondary	DyLight 405 donkey anti-rabbit	Jackson Immunoresearch 711-475-152	1:500
PV	all PV immunostaining	primary	goat anti-parvalbumin	Swant polyclonal antibody number PVG213	1:1,000
		secondary	Alexa 488 donkey anti-goat	Jackson Immunoresearch 705-545-147	1:500
VGLUT3	all VGLUT3 immunostaining	primary	guinea pig anti-VGLUT3	Chemicon polyclonal antibody, AB5421	1:10,000
		secondary	Alexa 488 donkey anti-guinea pig	Jackson Immunoresearch 706-545-148	1:500
VGAT	PV bouton counting only	primary	guinea pig anti-VGAT	Synaptic Systems polyclonal antibody, number 131 004	1:1,000
		secondary	Alexa 594 donkey anti-guinea-pig	Jackson Immunoresearch 706-585-148	1:500
cell fills	all except PV axon tracing	primary	biocytin-filled cell	Sigma-Aldrich B4261	8mM
		secondary	DyLight 405 streptavidin	Jackson Immunoresearch 016-470-084	1:200
cell fills	PV cell axon tracing only	primary	biocytin-filled cell	Sigma-Aldrich B4261	8mM
		secondary	Alexa 594 streptavidin	Jackson Immunoresearch 016-580-084	1:200

Table 2

Intrinsic properties of calb$^+$ and reelin$^+$ cells in juvenile control animals, adult sham control animals, and adult epileptic animals

See methods section and Fig 3 for descriptions of each of the measured intrinsic properties. Subscript 1 indicates the properties of the first spike in the most depolarized sweep. Properties with a Δ in front of them indicate a difference between the first spike and the subsequent 3 spikes in the most depolarized sweep. Note that because there were no differences in any of the measured parameters between epileptic and age-matched sham control animals, the right-hand column does not display the latter comparison.

Animal group (and number of animals)	**juvenile control (n=13)**		**adult sham control (n=6)**		**adult epileptic (n=8)**		**significant differences**	
Properties (see methods for descriptions)	**calbindin (n=21)**	**reelin (n=15)**	**calbindin (n=5)**	**reelin (n=11)**	**calbindin (n=−6)**	**reelin (n=18)**	**calb vs reelin**	**juvenile vs adult**
RMP (mV)	−62.3±0.5	−61.4±0.5	−59.8±1.9	−60.9±0.6	−63.3±1.3	−62.5±1.2		
R_{in} (MΩ)	65.3±3.0	52.6±5.3	82.3±7.0	69.2±6.0	80.1±10.8	64.9±4.4		
$Sag_{hyperpol}$ (mV)	2.6±0.1	2.9±0.2	2.5±0.5	3.5±0.3	2.7±0.2	3.2±0.3	p<0.0015	
τ_{sag} (ms)	12.1±0.2	27.3±0.9	45.4±5.3	31.3±4.3	60.5±7.0	40.7±8.1	p<0.0015	
$\tau_{membrane}$ (ms)	11.0±0.2	6.3±0.3	12.4±0.5	6.8±0.6	10.4±2.7	8.8±1.0	p<0.0015	
Rebound amplitude (mV)	2.3±0.1	3.0±0.2	1.8±0.4	3.4±0.2	2.0±0.7	3.2±0.3	p<0.0015	
Sag_{depol} (mV)	0.3±0.1	3.1±0.6	0.4±0.1	1.9±0.3	0.5±0.1	2.1±0.3	p<0.0015	
Rheobase (pA)	169±8	259±27	127±26	218±22	190±25	207±13	p<0.0015	
Delay to first spike (ms)	311±42	373±79	454±93	568±88	386±134	408±69		
Interspike interval (ms)	224±12	272±27	200±13	191±27	161±15	251±19		
Threshold (mV)	−43.7±0.6	−42.3±0.8	−41.0±0.8	41.1±1.2	−40.0±0.9	−42.3±1.2		
Spike Amplitude (mV from threshold)	75.6±1.4	70.0±1.5	75.5±1.9	68.0±2.5	67.2±4.1	74.3±2.3		
Spike half-width (ms)	0.70±0.02	0.64±0.02	0.63±0.02	0.57±0.03	0.59±0.04	0.70±0.03		
fAHP amplitude (mV from threshold)	−7.9±0.3	−8.5±0.4	−11.0±0.5	−10.3±0.8	−12.8±0.6	−9.8±0.5		p<0.0015
sAHP amplitude (mV from threshold)	−10.1±0.3	−11.3±0.3	−10.3±0.6	−11.6±0.7	−11.0±0.6	−12.7±0.7		
DAP amplitude (mV from fAHP)	0.2±0.1	1.2±0.3	0.7±0.2	2.5±0.6	0.9±0.2	3.6±0.4	p<0.0015	p<0.0015
$Threshold_1$ (mV)	−42.8±0.5	−40.8±1.0	−40.5±0.7	−40.3±1.1	−37.0±1.6	−40.8±1.2		
$Amplitude_1$ (mV)	72.3±1.2	65.1±1.7	72.0±2.0	64.0±2.4	61.9±.4	69.3±2.4		
$Halfwidth_1$ (ms)	0.67±0.03	0.59±0.02	0.58±0.02	0.55±0.03	0.60±0.05	0.68±0.04		
$fAHP_1$ (mV from threshold)	−9.4±0.3	−8.8±0.5	−12.3±0.5	−10.4±0.9	−14.4±0.9	−10.5±0.6	p<0.0015	p<0.0015
$sAHP_1$ (mV from threshold)	−8.4±0.3	−3.8±0.9	−9.2±0.7	−6.2±0.7	−9.3±0.5	−6.9±0.8	p<0.0015	

Animal group (and number of animals)	juvenile control (n=13)		adult sham control (n=6)		adult epileptic (n=8)		significant differences	
Properties (see methods for descriptions)	**calbindin (n=21)**	**reelin (n=15)**	**calbindin (n=5)**	**reelin (n=11)**	**calbindin (n=−6)**	**reelin (n=18)**	**calb vs reelin**	**juvenile vs adult**
DAP_1 (mV from $fAHP_1$)	1.0±0.2	5.2±0.7	−0.9±0.2	−0.5±0.3	−0.9±0.3	−0.2±0.2	p<0.0015	p<0.0015
Δ threshold (mV, compared to first spike)	0.72±0.38	−0.41±0.38	−0.70±0.37	0.47±0.30	−1.1±0.5	0.1±0.3	p<0.0015	
Δ spike amplitude (mV, compared to first spike)	1.2±0.3	2.5±0.5	1.0±0.6	1.1±0.6	2.3±0.7	1.6±0.4		
Δ halfwidth (ms, compared to first spike)	0.10±0.01	0.10±0.02	0.10±0.01	0.07±0.01	0.09±0.02	0.08±0.02		
ΔfAHP (mV, compared to first spike)	2.26±0.19	0.03±0.38	2.25±0.38	0.23±0.44	2.6±0.3	0.7±0.4	p<0.0015	
ΔsAHP (mV, compared to first spike)	0.8±0.2	−5.3±0.9	0.6±0.4	−3.3±0.7	0.4±0.2	−3.1±0.4	p<0.0015	
ΔDAP (mV, compared to first spike)	−0.8±0.2	−4.6±0.7	−1.6±0.4	1.0±0.5	−2.1±0.4	0.5±0.3		p<0.0015